



Frequency and voltage dependent electrical and dielectric properties of Al/*p*-Si semiconductor structures with GO interlayer



Niyazi Berk^a , Abdurrahman Turan^a, Şükrü Karataş^{a,b,*}

^a Department of Materials Science and Engineering, Kahramanmaraş Sutcu Imam University, Kahramanmaraş, 46100, Turkey

^b Department of Physics, Faculty of Sciences, Kahramanmaraş Sütçü İmam University, 46100, Kahramanmaraş, Turkey

ARTICLE INFO

Keywords:

Admittance measurements
High frequency
Dielectric properties
ac/dc conductivity
Electrical modulus

ABSTRACT

In this study, the electrical and dielectric properties of the Al/*p*-type Si semiconductor devices with graphene oxide interlayer at high frequencies ($f \geq 1$ MHz) were investigated in detail using capacitance-voltage and conductance-voltage measurements. All measurements were taken at room temperature between 1 MHz and 5 MHz with 1 MHz intervals. There was a decrease in capacitance and conductivity values due to the increase in frequency and voltage. The decrease of capacitance and conductance curves with increasing frequency and voltage is due to the existence of interface states. Also, the interface state densities and series resistance values were obtained from capacitance-voltage and conductance-voltage measurements. The interface state densities and series resistance values at 1 MHz and 5 MHz were obtained as 5.07×10^{14} – 9.11×10^{13} cm⁻² eV⁻¹ and 540 Ω–283 Ω, respectively. Furthermore, dielectric characteristics as known dielectric constant, dielectric loss, dielectric loss tangent, ac/dc electrical conductivity, and electrical modulus were obtained from capacitance-voltage and conductance-voltage measurements. It was seen that while dielectric constant, dielectric loss, dielectric loss tangent, ac/dc electrical conductivity values decreased with increasing frequency, electrical modulus values increased with increasing frequency. Thus, the experimental results show that the electrical and dielectric properties of graphene oxide interlayered Al/*p*-Si semiconductor devices change depending on frequency and voltage even at high frequencies.

1. Introduction

In general, the production of interlayer semiconductor devices is important to increase the charging or energy storage capacity in electronic devices. Because capacitance rises in structures with metal-semiconductor (MS) interfaces in proportion to the interface material's dielectric constant. The main purpose of using interface structures is to increase productivity by producing higher-performance semiconductor devices at lower costs. Because the interface layer prevents leakage current between both the metal and the semiconductor and thus the electric field in the semiconductor devices also remains constant. Thus, high-value dielectric interlayers instead of traditional oxide materials such as SiO₂, FeO, PbO (or derivatives), and SnO₂ at the interface to increase the capacitance would be a better choice for this purpose [1–6]. At the same time, the conduction mechanism and barrier height formation of MS structure can also be changed if a suitable interlayer is applied between metal and semiconductor structure. That is, it is clear that the interface layer significantly affects the stability, reliability and

performance of the device. Therefore, since graphene is the most studied and investigated nanomaterial with electrical, extraordinary mechanical, optical and surface properties, in this study, we used graphene oxide (GO) thin layer at the metal-semiconductor interface instead of traditional oxide layers. Especially today, graphene or GO has many applications in the electronics industry because it is a thin, transparent, durable and good conductive material. This means that graphene oxide-based semiconductor materials are successfully used in the electronics industry [7–11]. On the other hand, the fact that Andre Geim [12] and Kostya Novoselov [13] were awarded the Nobel Prize in 2004 for their successful research on GO clearly demonstrates how important the GO material is.

When the literature is examined, it is seen that different studies have been done on metal-semiconductor structures with interlayer [14–20]. However, detailed information on the electrical and dielectric properties of Al/GO/*p*-Si semiconductor devices with respect to frequency and voltage in the range of 1 MHz–5 MHz is quite scarce. Unlike our previous studies [14,15,17,21–24], in this study the electrical and dielectric

* Corresponding author. Department of Physics, Faculty of Sciences, Kahramanmaraş Sütçü İmam University, 46100, Kahramanmaraş, Turkey.
E-mail address: skaratas@ksu.edu.tr (Ş. Karataş).

properties GO interlayered Al/p-type Si semiconductor devices are defined as a function of both voltage and frequency at high frequencies ($1 \text{ MHz} \leq f \leq 5 \text{ MHz}$, by 1 MHz steps) using C - V , G/ω - V and R_S - V measurements. The frequency dependent interface states were obtained using the Hill-Coleman [25] method. First of all, we would like to point out that there is no study in the literature on the electrical and dielectric properties of GO interlayered Al/p-Si semiconductors at high frequencies. Studies on this subject are generally smaller than 1 MHz. Thus, this study is a new one and it is certain that it will make a very important contribution to the literature. The interface state densities (N_{SS}) and series resistance values (R_S) were obtained from C - V and G/ω - V measurements. Furthermore, dielectric characteristics as known dielectric constant (ϵ'), dielectric loss (ϵ''), dielectric loss tangent ($\tan\delta$), ac/dc electrical conductivity (σ_{ac} , σ_{dc}), and electrical modulus (M' , M'') were obtained from C - V and G/ω - V measurements. It was seen that while ϵ' , ϵ'' , $\tan\delta$, σ_{ac} and σ_{dc} values decreased with increasing frequency, M' , M'' values increased with increasing frequency. Thus, the experimental results show that the electrical and dielectric properties of GO interlayered Al/p-Si semiconductor devices change depending on frequency and voltage even at high frequencies.

2. Methods and materials

For this our study, we bought GO organic semiconductor powder from Fytronix and chemical solvents from Sigma-Aldrich. The Si wafer crystal that was utilized to produce the semiconductor structure has a resistance structure of $2-10 \Omega\text{-cm}$ and a thickness of $525 \mu\text{m}$ in the [100] direction. The wafer was chemically cleaned using the RCA [26] cleaning procedure. Detailed information about the RCA cleaning method was given in our previous study [27]. After, Al (99.999 percent) metal was evaporated at 10^{-6} Torr for ohmic contact (back contact) using a thermal evaporation equipment. The wafer was annealed using a dry nitrogen gas flow at 500°C for 3 min. After from ohmic contact, Si semiconductor wafer was cut into small pieces. The GO solution were prepared in chloroform. The semiconductor Si wafer front faces were coated GO solutions with spin speed of **1000 rpm for 30 s by spin coating method (6800 Spin Coater Series)**. Following these procedures, to make a rectifier Al metal contact with diameter of 1 mm ($=7.85 \times 10^{-3} \text{ cm}^2$) at 10^{-6} Torr pressure Al (%99.999 purity) metal was thermally evaporated on the surface of organic layer-semiconductor pieces, and as a result, the general diagram of the Al/GO/p-Si type semiconductor structure was obtained as shown in Fig. 1 (a). The Schematic representation and measurement system of the Al/GO/p-type Si semiconductor structure is shown in Fig. 1 (b). The energy band diagram of an Al/p-type Si structure with and without GO insulator layer is shown in Fig. 1 (c). In Fig. 1 (c); the terms Φ_s , Φ_m , δ , χ_s , E_V , E_F and E_C are the work function of the semiconductor, work function of the metal, thickness of the GO interfacial layer, electron affinity of the semiconductor, valence band of the semiconductor, Fermi energy, and conduction band of the semiconductor, respectively. At results, the frequency and voltage dependent C - V and G/ω - V measurements of Al/GO/p-type Si semiconductor structure were performed at high frequencies ($1 \text{ MHz} \leq f \leq 5 \text{ MHz}$, in 1 MHz steps) at room temperature by using ST2826/A High Frequency LCR Meter. The measurements were made on the converter board (IEEE-488 ac/dc) with the help of a computer.

3. Results and discussion

3.1. The C - V - f , G/ω - V - f and R_S - V - f electrical characteristics of Al/GO/p-Si semiconductor structure

Figs. 2 and 3 show the C - V and G/ω - V curves of the Al/GO/p-type Si semiconductor structure obtained as a function of voltage and frequency at room temperature and high frequencies ($1 \text{ MHz} \leq f \leq 5 \text{ MHz}$), respectively. As seen in Figs. 2 and 3, capacitance and conductance depend on both voltage and frequency; only the change is small at

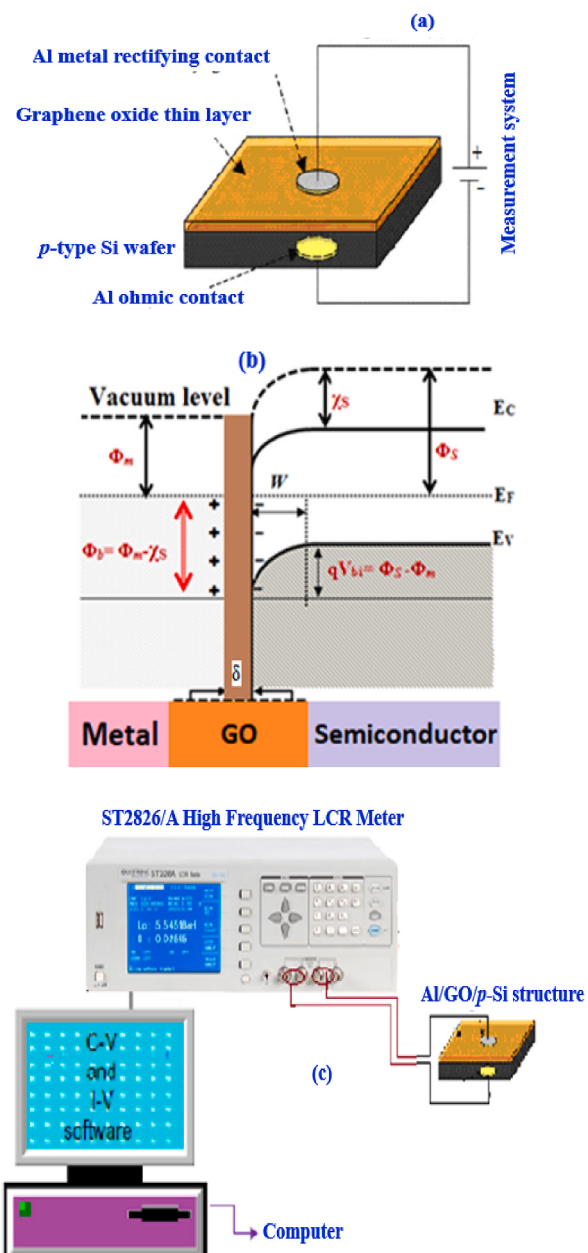


Fig. 1. (a) Schematic diagram of the Al/GO/p-type Si structure, (b) The measurement system of the Al/GO/p-type Si structure, (c) the energy band diagram of the Al/GO/p-type Si structure.

negative voltages, while the change is large at positive voltages. That is, at positive voltages, as can be seen, capacitance and conductance increase with decreasing frequency [28–36]. However, in the positive voltage region, capacitance (C) values give an abnormal peak for each frequency, while conductance (G/ω) values show an almost regular increase depending on the voltage. Also, this behavior of C and G/ω values generally indicates the presence of a continuous distribution of the interface states in semiconductor structures. Fig. 4 (a) and (b) show the changes in capacitance and frequency values of the Al/GO/p-Si type semiconductor structure in the range of $\pm 4.00 \text{ V}$ with steps of 0.50 V and 0.03 V, respectively. Similarly, Fig. 5 (a) and (b) also show the changes in capacitance and frequency values of the Al/GO/p-type Si semiconductor structure in the range of $\pm 4.00 \text{ V}$ with steps of 0.50 V and 0.03 V, respectively. As seen in Fig. 4(a and b) and Fig. 5(a and b), the capacitance and conductivity values of the semiconductor structure first decreased rapidly with the increase in frequency, but then remained

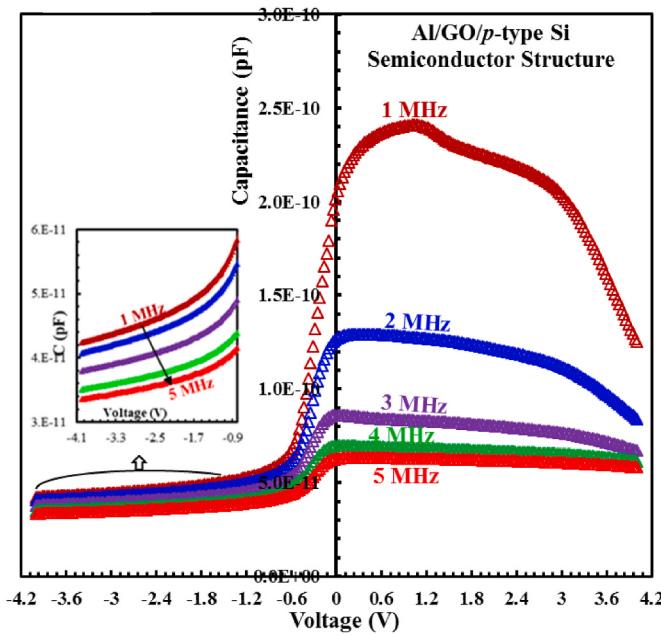


Fig. 2. Frequency dependent capacitance-voltage plots of the Al/GO/p-type Si structure.

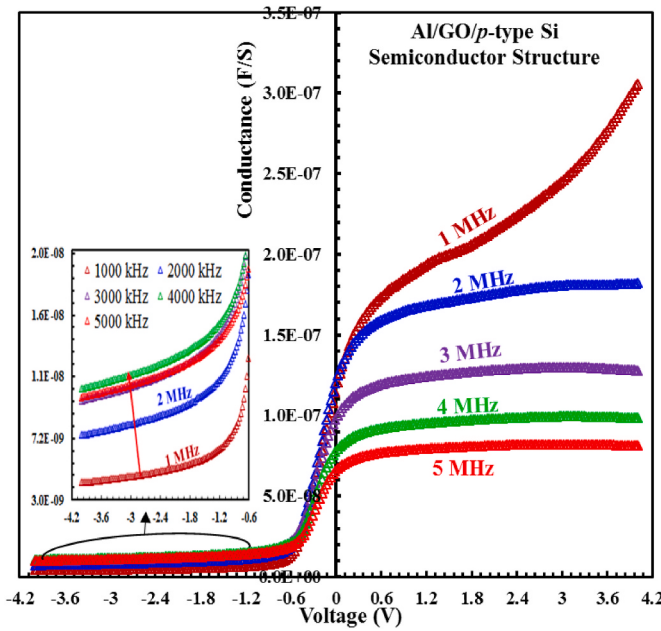


Fig. 3. Frequency dependent conductance-voltage plots of the Al/GO/p-type Si structure.

almost constant in the higher frequency ranges (from 4 MHz to 5 MHz). This means that in the frequency range of 1 MHz and 3 MHz, the interface states can follow the alternating current (a.c.) signal, but at higher frequencies (between 4 MHz and 5 MHz), the interface states cannot follow the a.c. signal [28–31,37]. Briefly, this phenomenon indicates that the Al/GO/p-Si type semiconductor structures have the ability to follow the AC signal of charge carriers even at high frequencies. However, at much higher frequencies, the charges cannot follow the AC signal due to the traps on the surface, which causes their presence to decrease.

At the same time, series resistance (R_S) is known to be a very important parameter that defines the performance of semiconductor

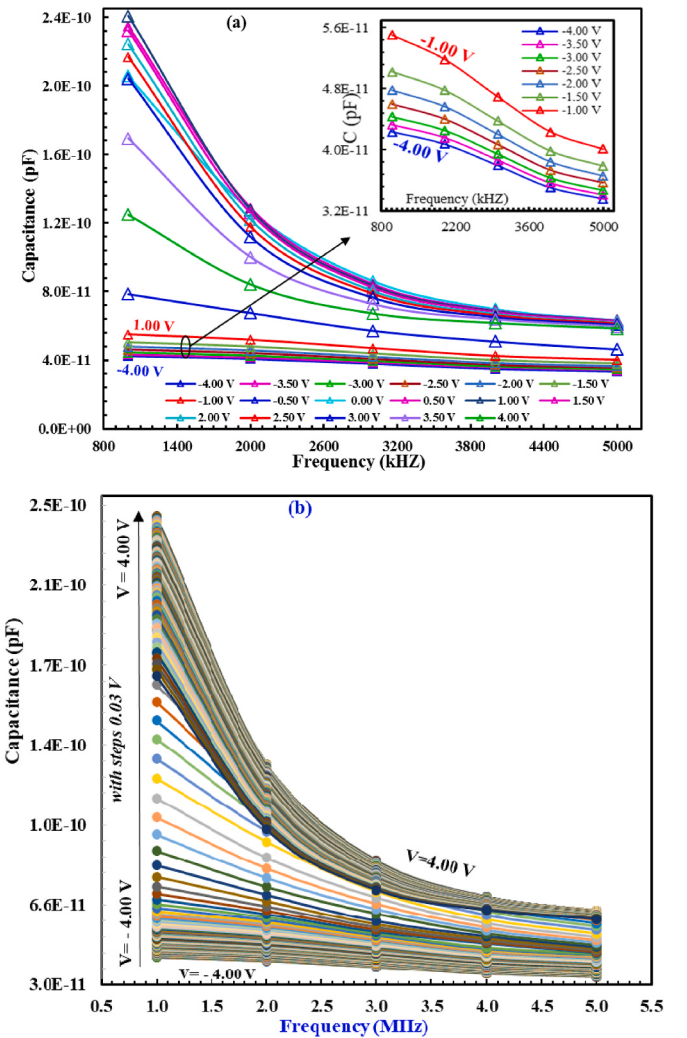


Fig. 4. Capacitance-frequency plots of the Al/GO/p-type Si structure in the range of ±4.00 V with steps of 0.50 V (a) and 0.03 V (b).

devices. Thus, Fig. 6 (a), (b), and (c) show the R_S - V and R_S - f curves in the frequency range of 1 MHz–5 MHz at the room temperature. The admittance (Y_{ma}) of semiconductor devices is equivalent to the admittance of the total circuit and can be written as [38];

$$Y_{ma} = [G_m + j\omega C_m] \quad (1)$$

here, the real part of the complex impedance ($Z = 1/Y$) represents the series resistance (R_S) and is given as;

$$R_S = \frac{G_m}{G_m^2 + (\omega C_m)^2} \quad (2)$$

in Eq. (2), C_m and G_m represent the C and G values measured for all voltage regions. The R_S - V curves obtained using Eq. (2) are shown in Fig. 6 (a). As seen in Fig. 6 (a), the R_S values give a peak at approximately −0.40 V at all frequencies ($1 \text{ MHz} \leq f \leq 5 \text{ MHz}$), and also the R_S values decreases as the frequency increases. The formation of peaks in R_S values is due to the change of interface traps or state distributions driven by the a.c. signal [39,40]. The R_S peak values of the Al/GO/p-type semiconductor structure in the range of $1 \text{ MHz} \leq f \leq 5 \text{ MHz}$ are given as 540 Ω, 421 Ω, 376 Ω, 324 Ω, and 283 Ω, respectively. This decrease in R_S values also causes C and G to vary with frequency. As can be seen in Fig. 6 (a), the R_S values are greatly affected by the applied frequency and voltage in all regions (inversion, depletion and accumulation), especially in the depletion region. We also obtained the series resistance

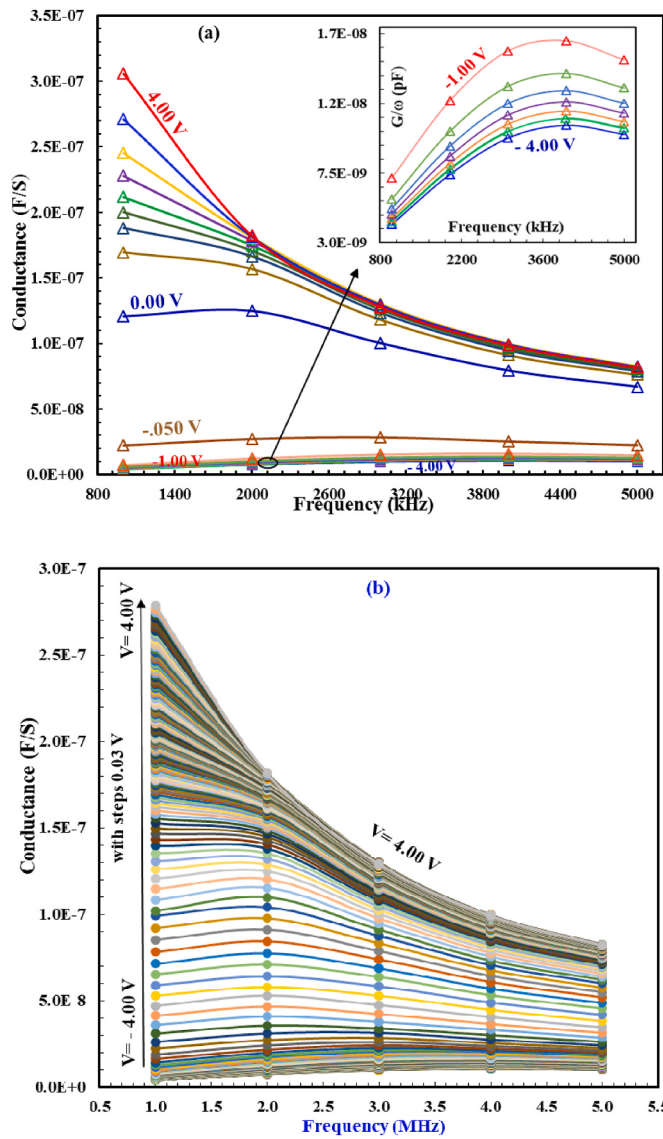


Fig. 5. Conductance–frequency plots of the Al/GO/p-type Si structure in the range of ± 4.00 V with steps of 0.50 V (a) and 0.03 V (b).

changes depending on the frequency at various voltages. Fig. 6 (b) and (c) show the changes in series resistance (R_S) and frequency values of the Al/GO/p-Si type semiconductor structure in the range of ± 4.00 V with steps of 0.50 V and 0.03 V, respectively. As seen in Fig. 6(b and c), the R_S values decreased as the frequency increased, but unlike the C and G, the decrease continued exponentially even at high frequencies. This means that the series resistance always varies strongly with frequency.

Additionally, we obtained the changes of interface state density (N_{SS}) with frequency using the Hill-Coleman method [25]. The interface state densities are important to define basic characteristics of semiconductor structures, since the properties of interfaced and non-interfaced MS structures are different. According to the Hill-Coleman model, N_{SS} is written as follows;

$$N_{SS} = \frac{2}{qA} \frac{\angle(G_C/\omega)_{\max}}{\angle((G_m/\omega)_{\max}/C_{ox})^2 + (1 - C_m/C_{ox})^2} \quad (3)$$

Here, A , ω , C_m , $(G/\omega)_{\max}$ and C_{ox} are diode area, angular frequency, capacitance, conductance, the insulator layer capacitance values, respectively. C_{ox} is obtained using the following equation,

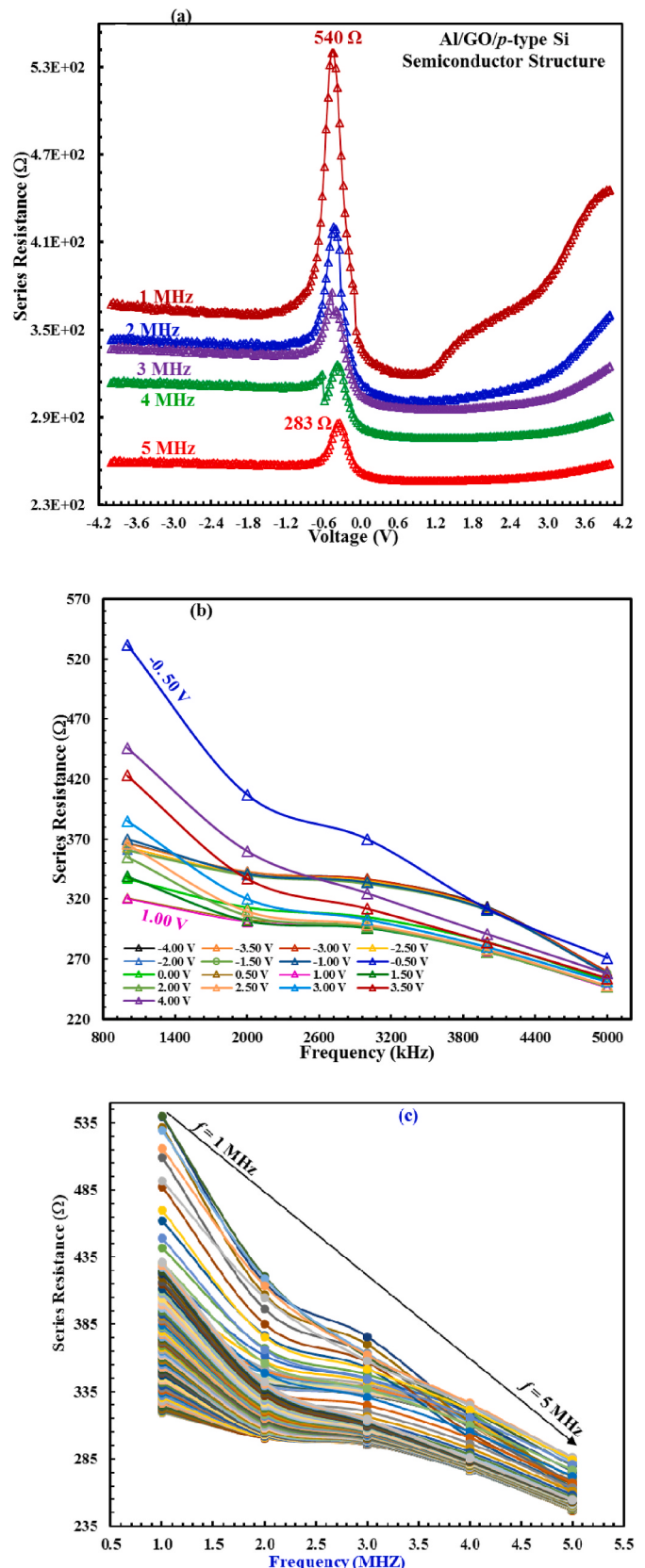


Fig. 6. (a) Frequency dependent series resistance–voltage plots of the Al/GO/p-type Si structure, (b) and (c) Series resistance–frequency plots in the range of ± 4.00 V with steps of 0.50 V and 0.03 V, respectively.

$$C_{ox} = \frac{\epsilon_i \epsilon_0 A}{d_{ox}} = C_{ma} \left(1 + \frac{G_m^2}{\omega^2 C_m^2} \right) \quad (4)$$

Fig. 7 shows the changes in N_{SS} values with frequency. As seen in Fig. 7, the N_{SS} values decrease periodically with increasing frequency, and these values are on the order of about $10^{14} \text{ cm}^{-1} \text{ eV}^{-1}$, and also these values reach a constant value between 4 MHz and 5 MHz. These situations indicate that the N_{SS} values are strongly dependent on frequency, thus causing an increase in the capacitance of the semiconductor structure.

3.2. The frequency-dependent dielectric characteristics of the Al/GO/p-Si semiconductor structure

Figs. 8–12 show the frequency dependent dielectric properties (ϵ' , ϵ'' , $\tan\delta$, σ_{ac} , σ_{dc} , $\ln\sigma_{ac}$, $\ln\sigma_{dc}$, M' , and M'') of the Al/GO/p-Si semiconductor structure. Dielectric materials are known as poor conductors of electricity because they have large energy band gaps and do not have free electrons as charge carriers. Dielectric materials are electrically insulating materials that can withstand strong electric fields without conducting current, often used in capacitors or radio frequency energy storage devices. That is, dielectric is known as an electrical insulator that can be polarized by the electric field. Thus, in this section, the dielectric characteristics (ϵ' , ϵ'' , $\tan\delta$, σ_{ac} , σ_{dc} , $\ln\sigma_{ac}$, $\ln\sigma_{dc}$, M' , and M'') of the Al/GO/p-Si semiconductor structure were investigated using C-V and G-V measurements at high frequencies ($1 \text{ MHz} \leq f \leq 5 \text{ MHz}$) and room temperature. The relative permittivity or complex dielectric constant/ coefficient (ϵ') corresponds directly to the capacitance (C) of the capacitor and is defined as the ratio of the permittivity of a substance to the permittivity of the free space. Thus, the electrical properties and quality of any material can be measured by its dielectric constant. The ϵ' of the material is written as [1–3,14,19,22,29,41–44];

$$\epsilon^*(\omega) = \epsilon'(\omega) - j\epsilon''(\omega) \quad (5)$$

Here, ϵ' and ϵ'' are real and imaginary values of complex permittivity, and also $\omega = 2\pi f$, and f is the frequency. As explained above (or in Eq. 5), the energy accumulated in the capacitor due to the applied electric field is measured by ϵ' . Furthermore, the symbol ϵ'' is usually used to describe the state of energy distributed in a dielectric material. Thus, the ϵ' and ϵ'' values in the case of admittance calculates can be expressed as follows [19,45,46];

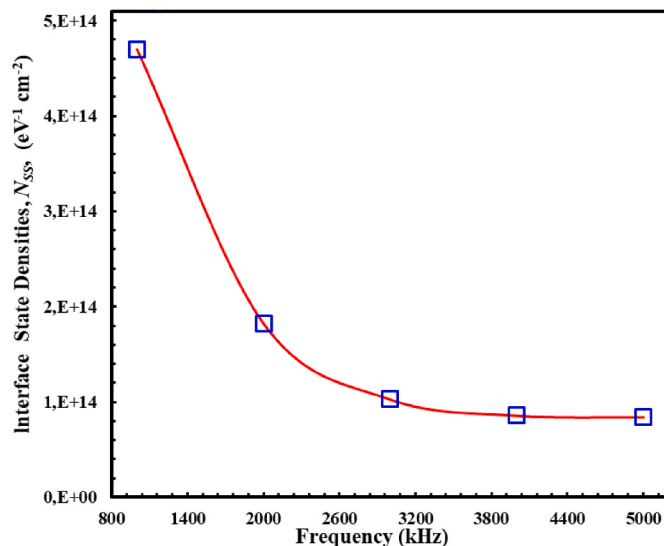


Fig. 7. Frequency-dependent interface states density of the Al/GO/p-type Si structure.

$$\epsilon' = \frac{C_m}{C_0} \quad (6)$$

$$\epsilon'' = \frac{G_m d_{ox}}{A \epsilon_0 \omega} = \frac{G_m}{\omega C_0} \quad (7)$$

Also in Eq. (5), the ratio of the imaginary part to the real part gives the value $\tan\delta$, which is known as the amount of energy lost. That is, loss tangent ($\tan\delta$);

$$\tan \delta = \frac{\epsilon''}{\epsilon'} = \frac{G}{\omega C_m} \quad (8)$$

In above equations, $C_0 = (\epsilon_0 A / d_{ox})$; A is contact's area ($= 0.00785 \text{ cm}^2$), d_{ox} is insulator layer thickness and ϵ_0 is $8.85 \times 10^{-14} \text{ F/cm}$ (free space charge permittivity). It is also an important parameter in electrical conductivity (σ_{ac} or σ_{dc}) in dielectric materials and gives the electric current that the material can carry. Thus, a.c electrical conductivity (σ_{ac}) and d.c electrical conductivity (σ_{dc}) can be written as follows, respectively [45–48];

$$\sigma_{ac} = \omega \epsilon_0 \epsilon' \tan \delta \quad (9)$$

$$\sigma_{dc} = (\omega \epsilon_0 \epsilon' \tan \delta) / (4\pi) \quad (10)$$

For Al/GO/p-Si semiconductor structure, using Eqs. (6)–(11), Fig. 8 (a, b) shows the frequency dependent of the ϵ' and ϵ'' values, Fig. 9 shows the frequency dependent $\tan\delta$ values, Fig. 10 (a, b) shows the frequency dependent electrical conductivity (σ_{ac} and σ_{dc}) values, and finally Fig. 11 (a, b) shows frequency dependent $\ln\sigma_{ac}$ and $\ln\sigma_{dc}$ values, respectively. As seen in Figs. 6–11, the dielectric values of the Al/GO/p-Si structure are highly dependent on the frequency even high frequencies and these values decrease with the increase in frequency. However, in Fig. 11 (a, b) $\ln\sigma_{ac}$ and $\ln\sigma_{dc}$ values shows a linear situation depending on the frequency. This decrease in dielectric properties depending on frequency is an expected situation for semiconductor structures. Because the decrease in dielectric properties (ϵ' , ϵ'' , $\tan\delta$, σ_{ac} , σ_{dc} , $\ln\sigma_{ac}$, $\ln\sigma_{dc}$) at high frequencies for the Al/GO/p-Si structure means that there is a polarization mechanism at the interface [45–48]. Also, the decrease in dielectric properties with increasing frequency can also be explained by the fact that the interface dipoles have less time to orient themselves in the direction of the applied electric field. Furthermore, as seen in Fig. 11 (a) and 11 (b), there is a linear relationship between logarithmic conductivity ($\ln\sigma_{ac}$ and $\ln\sigma_{dc}$) and frequency, and the slopes

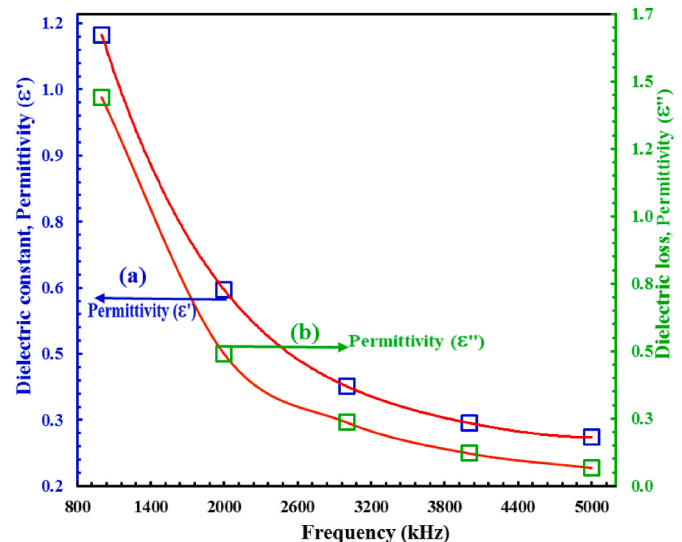


Fig. 8. Frequency-dependent (a) dielectric constant (ϵ') and (b) dielectric loss (ϵ'') of Al/GO/p-type Si structure.

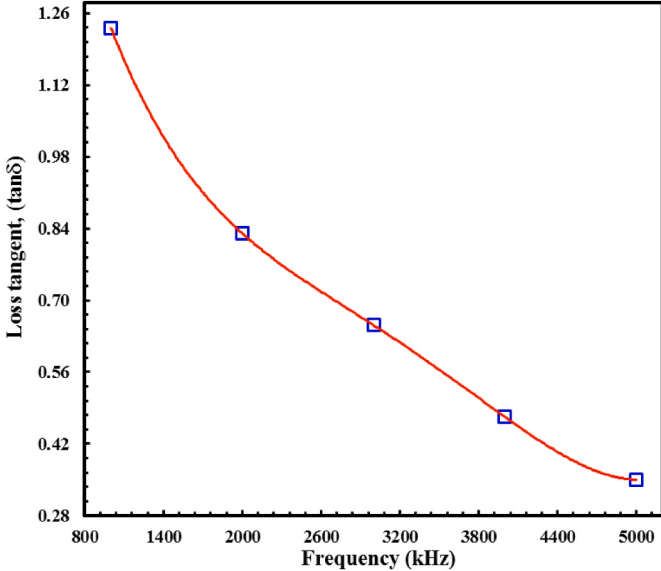


Fig. 9. Frequency dependent change of loss tangent ($\tan\delta$) of the Al/PTCDA/p-Si structure.

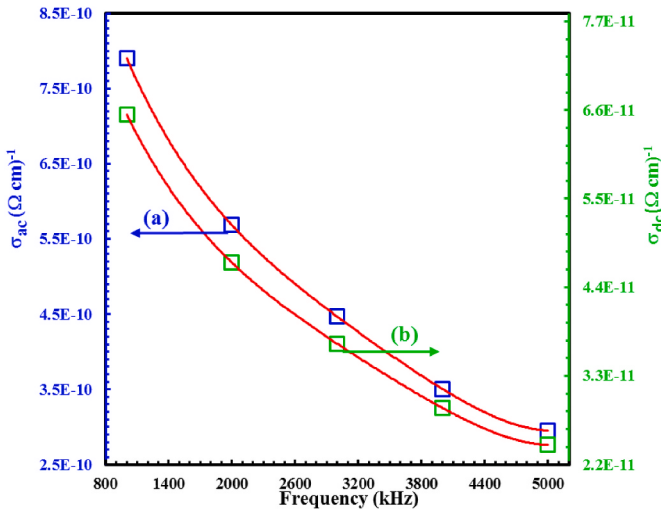


Fig. 10. Frequency dependent change of electrical conductivity of the Al/PTCDA/p-Si structure; (a) σ_{ac} and (b) σ_{dc} .

of these graphs are less than 1. These states demonstrate that the Al/GO/p-Si structure's conductivity behavior changes in different frequency regions and depends on the polarization and series resistance of the structure [49,50]. In addition, another important technique to investigate the electrical transport mechanism for dielectric materials and understand how it affects local dielectric relaxation is to measure the complex dielectric modulus. Fig. 12a and b show the frequency dependent changes of the real (M') and imaginary (M'') parts of the electric module, respectively. Accordingly, the real M' and imaginary M'' parts of the electric module can be calculated from ϵ' and ϵ'' as follows [51–53];

$$M' = \frac{1}{\epsilon^*} = M' + jM'' = \frac{\epsilon'}{(\epsilon'^2 + \epsilon''^2)} + j \frac{\epsilon''}{(\epsilon'^2 + \epsilon''^2)} \quad (11)$$

Thus, M' and M'' can be calculated using the following equations;

$$M'(\omega) = \frac{\epsilon'}{(\epsilon'^2 + \epsilon''^2)} \quad (12)$$

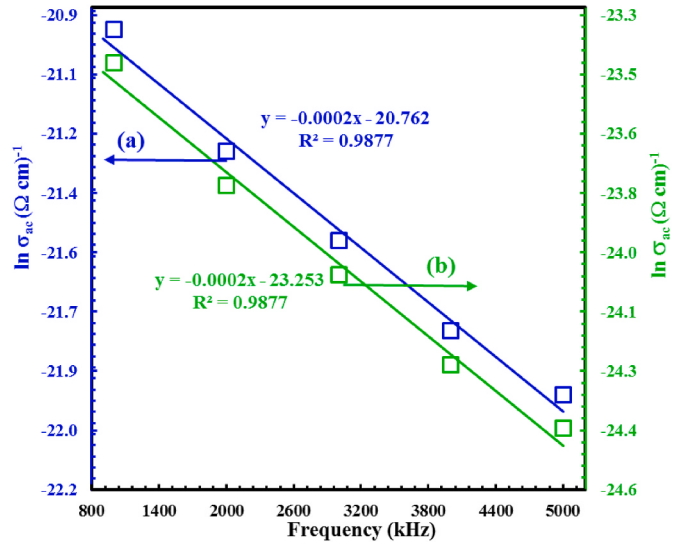


Fig. 11. Frequency dependent change of (a) $\ln \sigma_{ac}$ and (b) $\ln \sigma_{dc}$ values of the Al/PTCDA/p-Si structure.

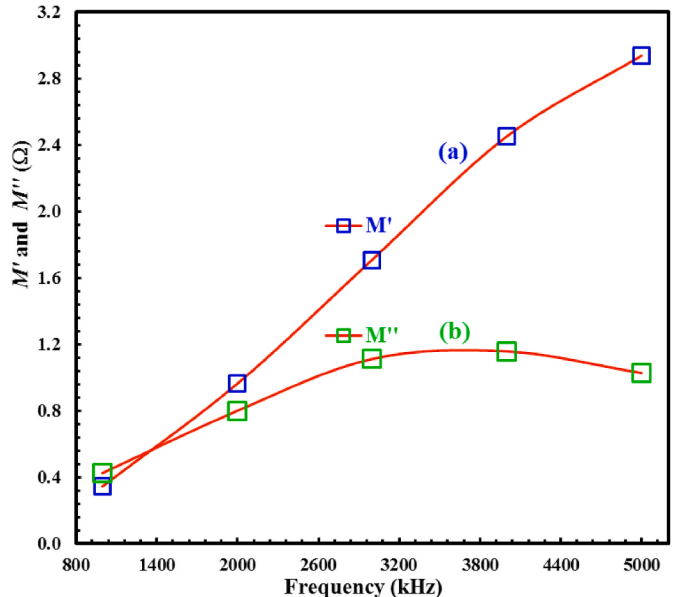


Fig. 12. Frequency dependent change of complex dielectric modulus of the Al/PTCDA/p-Si structure; (a) M' and (b) M'' values.

$$M''(\omega) = \frac{\epsilon''}{(\epsilon'^2 + \epsilon''^2)} \quad (13)$$

As seen in Fig. 12a and b, both M' and M'' values increase with increasing frequency values. This means that the increase in M and M'' could be due to the lack of a restoring force that governs the mobility of charge carriers under the influence of an induced electric field [51,52]. Moreover, this behavior also ensures long-term mobility of charge carriers [51–55].

4. Conclusions

In this our study, the electrical and dielectric parameters of Al/GO/p-Si semiconductor structures at high frequencies ($f \geq 1$ MHz) were investigated in detail using C-V and G/ ω -V measurements. It was observed that the investigated electrical (N_{SS} and R_S) and dielectric (ϵ' , ϵ'' , $\tan\delta$, σ_{ac} , σ_{dc} , $\ln \sigma_{ac}$, $\ln \sigma_{dc}$, M' , and M'') parameters were strongly

dependent on frequency and voltage, especially in the depletion and accumulation regions. The decrease in C and G/ω -values at increasing frequencies depending on frequency and voltage is due to the presence of graphene oxide at the metal semiconductor interface. The series resistance-voltage (R_s - V) curves give a decreasing peak with increasing frequency and the interface state density is also seen to decrease (from 5.07×10^{14} to $9.11 \times 10^{13} \text{ cm}^{-2} \text{ eV}^{-1}$) exponentially with frequency. This state shows that for the Al/GO/p-Si structure, the interface states can follow the alternating current (a.c) signal even at higher frequencies ($f \geq 1 \text{ MHz}$). Furthermore, experimental results showed that while the frequency dependent dielectric values (ϵ' , ϵ'' , $\tan\delta$, σ_{ac} , σ_{dc} , $\ln\sigma_{ac}$, and $\ln\sigma_{dc}$) decreased with increasing frequency, the complex dielectric modulus (M' and M'') values also increased with increasing frequency. That is, the exponential decrease of ϵ' , ϵ'' , $\tan\delta$, σ_{ac} , σ_{dc} , $\ln\sigma_{ac}$, and $\ln\sigma_{dc}$ values with increasing frequency and the increase of M' and M'' values mean that the balance of charge carriers is disrupted by the effect of the applied external electric field. This shows that the behavior is also dependent on the polarization due to the applied electric field. These experimental findings indicate that the presence of GO layer between Al/p-Si metal semiconductors can improve the quality of the semiconductor. As conclusion, we can say that Al/GO/p-type Si structure is suitable for high quality electronic, capacitor and optoelectronic applications.

CRedit authorship contribution statement

Niyazi Berk: Resources, Investigation, Formal analysis, Data curation. **Abdurrahman Turan:** Methodology, Investigation, Formal analysis, Data curation. **Şükrü Karataş:** Writing – review & editing, Writing – original draft, Supervision, Methodology, Investigation, Formal analysis, Data curation, Conceptualization.

Declaration of competing interest

The authors declare that they have no known competing financial interests or personal relationships that could have appeared to influence the work reported in this paper.

Acknowledgement

This work was supported by Kahramanmaraş Sütçü Imam University Scientific Research Project (Project number: 2025/2-1 YLS). We would like to thank Kahramanmaraş Sütçü Imam University for financial support of the research program.

Data availability

Data will be made available on request.

References

- [1] E.H. Rhoderick, R.H. Williams, *Metal-Semiconductor Contacts*, 2nd edn., Clarendon, Oxford, 1988.
- [2] S.M. Sze, K. Ng Kwok, *Physics of Semiconductor Devices*, third ed., John Wiley & Sons, New Jersey, 2007.
- [3] B.L. Sharma, *Metal-semiconductor Schottky Barrier Junctions and Their Applications*, Plenum Press, New York, 1984.
- [4] Ş. Karataş, A. Türüt, Ş. Altindal, *Rad. Phys. Chem.* 78 (2009) 130.
- [5] M. Yürekli, A.F. Özdemir, Ş. Altindal, *J. Mater. Sci. Mater. Electron.* 35 (2024) 422.
- [6] S.J.-D. Hwang, C.-S. Li, C.-Y. Chang, *Alloys Compd* 960 (2023) 170508.
- [7] N. Berk, H. Seymen, İ. Orak, Ş. Karataş, *J. Phys. Chem. Solid.* 160 (2022) 110348.
- [8] A. Peigney, C. Laurent, E. Flahaut, R.R. Bacsa, A. Rousset, *Carbon* 39 (2001) 507.
- [9] D. Khlaifia, M. Aouassa, L. Torrisi, M. Cutroneo, A.K. Aladim, I. Berbezier, *Phys. B Condens. Matter* 706 (2025) 417133.
- [10] I. Tiye, M. Yazıcı, M.H. Alma, Ş. Karataş, *Journal of Composite Materials* 53 (11) (2019) 1541.
- [11] S. Stankovich, D.A. Dikin, G.H.B. Dommett, K.M. Kohlhaas, E.J. Zimney, E. A. Stach, R.D. Piner, S.T. Nguyen, R.S. Ruoff, *Nature* 442 (2006) 282.
- [12] A.K. Geim, K.S. Novoselov, *Nat. Mater.* 6 (2007) 183.
- [13] K.S. Novoselov, A.K. Geim, S.V. Morozov, D. Jiang, M.I. Katsnelson, I. V. Grigorieva, S.V. Dubonos, A.A. Firsov, *Nature* 438 (2005) 197.
- [14] A. Kilçik, N. Berk, H. Seymen, Ş. Karataş, *J. Mater. Sci. Mater. Electron.* 32 (2021) 7913.
- [15] Ş. Karataş, M.G. Aydin, H. Özerli, *J. Alloys Compd.* 689 (2016) 1068.
- [16] Z. Çaldıran, M. Sinforoğlu, Ö. Metin, Ş. Aydogan, K. Meral, *J. Alloys Compd.* 631 (2015) 261.
- [17] Ş. Karataş, N. Berk, *Opt. Mater.* 126 (2022) 112231.
- [18] Y. Wang, S. Yang, D.R. Lambada, S. Shafique, *Sens. Actuators, A* 314 (2020) 112232.
- [19] Ş. Karataş, J. Sandw. Struct. Mater. 23 (2021) 739.
- [20] M. Sharifi, N. Naderi, P. Fallahazad, M.J. Eshraghi, *Sens. Actuator A* 310 (2020) 112065.
- [21] H. Seymen, N. Berk, H. Özerli, Ş. Karataş, *Phys. B Condens. Matter* 685 (2024) 416026.
- [22] Ş. Karataş, F. Canlı, F. Yakuphanoğlu, *Phys. B Condens. Matter* 677 (2024) 415725.
- [23] Ş. Karataş, A. Ak, *Phys. Scri.* 99 (2024) 065905.
- [24] H. Seymen, Ş. Karataş, *Mater. Chem. Phys.* 310 (2023) 128449.
- [25] W.A. Hill, C.C. Coleman, *Solid State Electron.* 23 (1980) 987.
- [26] <https://www.inrf.uci.edu/wordpress/wp-content/uploads/sop-wet-silicon-rca-1.pdf>.
- [27] Ş. Karataş, A. Türüt, *Microelectron. Reliab.* 50 (2010) 351.
- [28] H.I. Efkere, A. Barkhordari, B. Marmiroli, B. Sartori, S. Özçelik, G.P. Givi, Ş. Altindal, Y.A. Kalandaragh, *Phys. Scri.* 99 (2024) 055967.
- [29] S. Bengi, H.G. Çetinkaya, Ş. Altindal, S. Zeyrek, *J. Electron. Mater.* 53 (2024) 5606.
- [30] Ç.S. Güçlü, E.E. Tanrikulu, M. Ulusoy, Y.A. Kalandaragh, Ş. Altindal, *J. Mater. Sci. Mater. Electron.* 35 (2024) 348.
- [31] Ş. Karataş, F. Yakuphanoğlu, F.M. Amanullah, *J. Phys. Chem. Solid.* 73 (2012) 46.
- [32] Ş. Karataş, *J. Mater. Sci. Mater. Electron.* 32 (2021) 707.
- [33] Ş. Karataş, *J. Mater. Electron. Devic.* 4 (2020) 11.
- [34] H. Özerli, İ. Karteri, Ş. Karataş, Ş. Altindal, *Mater. Res. Bull.* 53 (2014) 211.
- [35] H. Durmuş, H.Ş. Kilç, S.Y. Gezgin, Ş. Karataş, *Silicon* 10 (2018) 361.
- [36] Ş. Karataş, *J. Mater. Sci. Mater. Electron.* 32 (2020) 707.
- [37] H. Tecimer, H. Uslu, Z.A. Alahmed, F. Yakuphanoğlu, Ş. Altindal, *Composites, Part B* 57 (2014) 25.
- [38] E.H. Nicollian, A. Goetzberger, *Bell Syst. Tech. J.* 46 (1967) 1055.
- [39] I. Gümrüs, Ş. Aydogan, *Sensors and Actuators A*, vol. 331, 2021 112989.
- [40] M. Koca, Z. Kudaş, D. Ekinci, Ş. Aydogan, *Mater. Sci. Semicond. Process.* 121 (2021) 105436.
- [41] Ş. Altindal, A. Barkhordari, Y. Azizian-Kalandaragh, B.S. Çevrimli, H. R. Mashayekhi, *Mater. Sci. Semicond. Process.* 147 (2022) 106754.
- [42] R.O. Ocaya, A.G. Al-Shehmi, Ş. Karataş, A. Tataroğlu, A. Dere, A.A. Al-Ghamdi, F. Yakuphanoğlu, *Opt. Mater.* 150 (2024) 115320.
- [43] A. Karabulut, A. Türüt, Ş. Karataş, *J. Mol. Struct.* 1157 (2018) 513.
- [44] Ş. Karataş, Z. Kara, *Microelectron. Reliab.* 51 (2011) 2205.
- [45] P. Pissis, A. Kyritsis, *Solid State Ionics* 97 (1997) 105.
- [46] T. Çakıcı, A. Ajjaq, A.O. Çağırtekin, Ö. Barın, M. Özdal, S. Acar, *Appl. Surf. Sci.* 631 (2023) 157522.
- [47] Ö. Sevgili, Y.A. Kalandaragh, Ş. Altindal, *B. Physica, Phys. Condens. Matter* 587 (2020) 412122.
- [48] N. Delen, Ş.A. Yerişkin, A. Özbay, İ. Taşçıoğlu, *Physica B: Cond. Mat.* 665 (2023) 415031.
- [49] A.E. Tezcan, S.A. Hameed, A.F. Vahid, M. Ulusoy, Ş. Altindal, *Physica B: cond. Mat.* 684 (2024) 415959.
- [50] E.E. Tanrikulu, Ş. Altindal Yerişkin, *B. Physica, Phys. Condens. Matter* 623 (2021) 413345.
- [51] S. Amdouni, M. Aouassa, M. Bouabdellaoui, A.K. Aladim, M. Yahyaoui, *Vacuum* 224 (2024) 113191.
- [52] A. Bobby, N. Shiawoti, P.M. Sarun, S. Verma, K. Asokan, B.K. Antony, *Curr. Appl. Phys.* 15 (2015) 1500.
- [53] K.M.A. Saron, M. Aouassa, N.K. Hassan, M.G. Moustafa, T. Kallel, A.K. Aladim, M. Ibrahim, S.A. Algarni, M. Bouabdellaoui, I. Berbezier, *Phys. B Condens. Matter* 704 (2025) 417061.
- [54] A.B. Uluş, A. Tataroğlu, *Silicon* 10 (2018) 2071–2077.
- [55] N. Shiawoti, A. Bobby, K. Asokan, B. Antony, *Mater. Sci. Semicond. Process.* 42 (2016) 378.